The EMBO Journal (2011) 30, 2793–2804 | © 2011 European Molecular Biology Organization | All Rights Reserved 0261-4189/11
www.embojournal.org

THE EMBO JOURNAL

A synthetic prestin reveals protein domains and molecular operation of outer hair cell piezoelectricity

Thorsten J Schaechinger[1], Dmitry Gorbunov[2], Christian R Halaszovich[2], Tobias Moser[3], Sebastian Kügler[4], Bernd Fakler[1,5] and Dominik Oliver[2,*]

[1]Institute of Physiology, University of Freiburg, Freiburg, Germany, [2]Department of Neurophysiology, Institute of Physiology and Pathophysiology, Philipps-University, Marburg, Germany, [3]InnerEarLab, Department of Otolaryngology and Center for Molecular Physiology of the Brain, University of Göttingen, Goettingen, Germany, [4]Department of Neurology, University of Göttingen, Medical School, Göttingen, Germany and [5]BIOSS Centre for Biological Signaling Studies, University of Freiburg, Freiburg, Germany

Prestin, a transporter-like protein of the SLC26A family, acts as a piezoelectric transducer that mediates the fast electromotility of outer hair cells required for cochlear amplification and auditory acuity in mammals. Non-mammalian prestin orthologues are anion transporters without piezoelectric activity. Here, we generated synthetic prestin (SynPres), a chimera of mammalian and non-mammalian prestin exhibiting both, piezoelectric properties and anion transport. SynPres delineates two distinct domains in the protein's transmembrane core that are necessary and sufficient for generating electromotility and associated non-linear charge movement (NLC). Functional analysis of SynPres showed that the amplitude of NLC and hence electromotility are determined by the transport of monovalent anions. Thus, prestin-mediated electromotility is a dual-step process: transport of anions by an alternate access cycle, followed by an anion-dependent transition generating electromotility. The findings define structural and functional determinants of prestin's piezoelectric activity and indicate that the electromechanical process evolved from the ancestral transport mechanism.

The EMBO Journal (2011) **30,** 2793–2804. doi:10.1038/emboj.2011.202; Published online 24 June 2011
Subject Categories: membranes & transport; neuroscience
Keywords: anion transport; cochlea; outer hair cell; prestin; SLC26

Introduction

Hearing in vertebrates involves an active amplification process in the auditory periphery that determines the exquisite sensitivity and frequency selectivity (Dallos, 2008; Hudspeth, 2008). In mammals, this 'cochlear amplification' is provided by the outer hair cells (OHCs), a distinct and structurally specialized population of mechanosensory hair cells that change their length in response to changes in membrane potential (Brownell *et al*, 1985; Ashmore, 1987). These fast voltage-dependent cellular length changes, termed electromotility, can operate at frequencies of at least 70 kHz (Frank *et al*, 1999) (i.e. ultrasonic frequencies, e.g. in bats) and are required for amplification of the sound-induced vibrations in the cochlea (Dallos *et al*, 2008).

Mechanistically, the electromotility of OHCs is similar to piezoelectric materials that change dimensions under the influence of voltage (Ashmore, 2008). As the elementary molecular motor generating electromotility, Dallos and co-workers identified prestin (SLC26A5), a member of the SLC26 family of anion exchangers (Zheng *et al*, 2000). Prestin is thought to act as an area motor by alternating between two major conformations that occupy different cross-sectional areas within the membrane and were, therefore, termed 'long' and 'short states' (Iwasa, 2001; Dallos and Fakler, 2002). Joint conformational transitions of the tightly packed prestin motors in the plasma membrane of the OHC lead to length changes of the whole cell (models reviewed by Dallos and Fakler, 2002; Ashmore, 2008). The distribution between long and short conformations is immediately voltage dependent, which inevitably requires a mobile charged particle acting as a voltage sensor (Bezanilla, 2008). In fact, fast voltage-dependent charge movement is a hallmark of prestin that can be experimentally assessed as a non-linear capacitance (NLC) (Santos-Sacchi, 1991; Dallos and Fakler, 2002). Because of its straight accessibility and precise quantification, NLC is routinely used as a surrogate measure for electromotility (Figure 1A).

Aside from the basic biophysical characteristics, little is known about structural and molecular details of prestin's function. We and others have previously demonstrated that NLC, and hence electromotility, is critically dependent on monovalent intracellular anions, in particular chloride (Cl^-) (Oliver *et al*, 2001; Rybalchenko and Santos-Sacchi, 2003, 2008; Santos-Sacchi *et al*, 2006), suggesting a mechanistic link between electromotility and the anion transport observed with related SLC26 transporters. In fact, analysis of the phylogenetic relationship of vertebrate SLC26A5 orthologues (Franchini and Elgoyhen, 2006; Okoruwa *et al*, 2008) indicated that mammalian prestin evolved from an anion transporter present in pre-mammalian ancestors. Thus, we recently found that non-mammalian SLC26A5 orthologues are bona fide electrogenic anion antiporters (Schaechinger and Oliver, 2007), which, however, fail to generate fast NLC and electromotility (Albert *et al*, 2007; Tan *et al*, 2011). Vice versa, mammalian prestin lacks electrically detectable transport activity (Schaechinger and Oliver, 2007; Figure 1A and B).

*Corresponding author. Department of Neurophysiology, Institute of Physiology and Pathophysiology, Philipps-University, Deutschhausstrasse 2, 35037 Marburg, Germany.
Tel.: +49 6421 286 6444; Fax: +49 6421 286 2306;
E-mail: oliverd@staff.uni-marburg.de

Received: 28 January 2011; accepted: 24 May 2011; published online: 24 June 2011

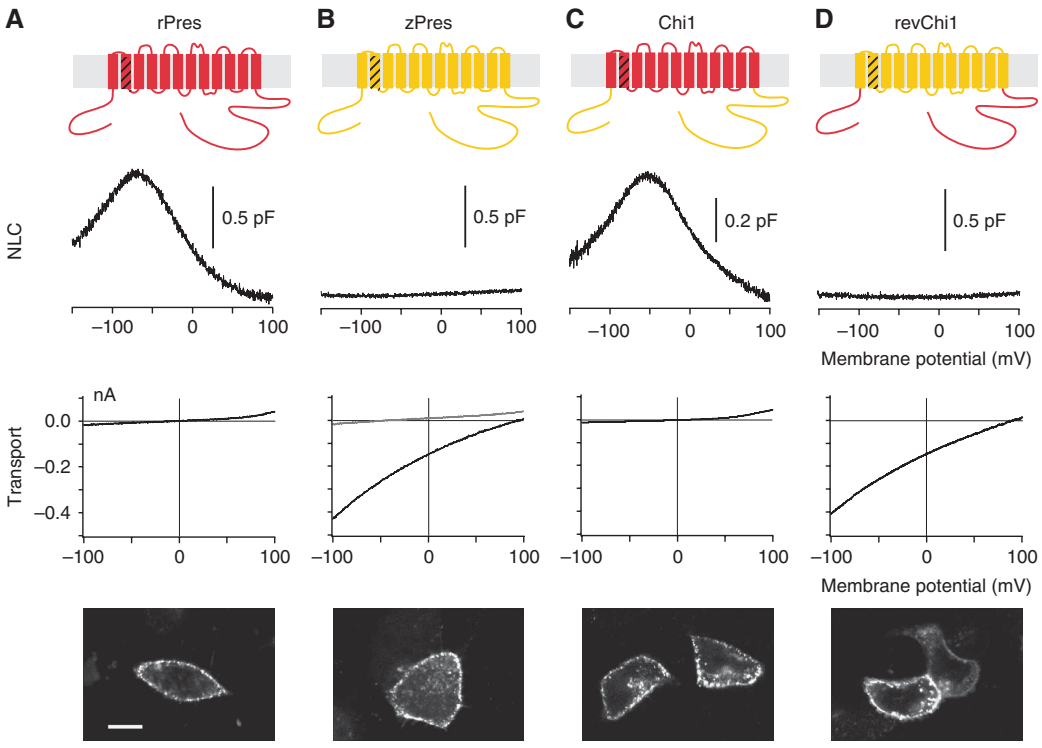

Figure 1 Electromotility-associated NLC and transport are determined by the transmembrane core region of mammalian and non-mammalian prestin. (**A**–**D**) NLC and electrogenic anion transport recorded from whole-cell voltage-clamped CHO cells expressing rPres (**A**), zPres (**B**), Chi1 (**C**), or revChi1 (**D**). Intracellular solution contained 160 mM Cl^- for NLC recordings or 10 mM oxalate and 10 mM Cl^- for transport current measurements. Traces for NLC and transport are each representative for more than five experiments; grey trace in (**B**, transport measurement) is with oxalate omitted from the intracellular solution. Plasma membrane localization of the constructs is shown by representative confocal images from CHO cells (lower panels; scale bar for all images, 10 μm). Cartoons (upper panels) represent the suggested 12 TM topology of prestin (Oliver *et al*, 2001; Zheng *et al*, 2001); for alternative topology model, see Navaratnam *et al* (2005); shaded domain indicates SLC26 signature motif.

In this study, we took advantage of the functional divergence between mammalian and non-mammalian orthologues for analysing prestin-mediated fast electromotility. Using chimeras between rat (rPres) and zebrafish (zPres) orthologues, we generated a synthetic prestin (SynPres) protein that combines piezoelectric properties with robust electrogenic anion transport and thus provides a novel experimental paradigm for direct investigation of the mechanistic relation between fast electromotility and anion transport.

Results

Structural determinants of electromotility—generation of SynPres

For elucidating the protein domains that underlie electromotility and NLC, its electrical signature, in mammalian prestin, we generated chimeras between the prestin orthologues of rat (rPres) and zebrafish (zPres). Both proteins are highly homologous (see Supplementary Figure S1) and exhibit identical overall topologies, but are largely different with respect to their functional properties observed in cultured CHO cells upon heterologous expression (Albert *et al*, 2007; Schaechinger and Oliver, 2007). Thus, rPres displays robust electromotility and NLC, but fails to transport anions across the plasma membrane (Figure 1A); in contrast, zPres does not show fast NLC, but operates as an electrogenic anion transporter that effectively exchanges Cl^- for divalent anions such as oxalate, giving rise to large transport currents (Figure 1B).

Initially, we switched the hydrophobic core region thought to comprise 12 transmembrane domains (Oliver *et al*, 2001; Zheng *et al*, 2001) between rPres and zPres (Figure 1, upper panel). As shown in Figure 1C, the chimera (Chi1) placing the core of rPres between the cytoplasmic N- and C-termini of zPres lacked electrogenic anion transport activity, but displayed robust NLC with voltage-dependent characteristics very similar to rPres. The voltage at maximal NLC ($V_{1/2}$) and the steepness of voltage dependence (α) obtained from fits of the derivative of a Boltzmann function to the data were $V_{1/2} = -31.9 \pm 14.8$ mV (mean ± s.d., $n = 11$) and -77.7 ± 16.0 mV ($n = 20$), and $\alpha = 38.0 \pm 3.0$ mV and 38.6 ± 2.6 mV, for Chi1 and rPres, respectively. Similarly, the inverse chimera where the N- and C-termini of rPres flanked the core region of zPres (revChi1) reproduced the properties of the non-mammalian zPres as indicated by electrogenic transport and complete lack of NLC (Figure 1D). These data indicated that NLC and anion transport are mediated by the transmembrane core, while the cytoplasmic termini are not directly involved.

Consequently, the next series of constructs probed distinct domains within the transmembrane core for their functional significance, with a first focus on its N-terminal end. This region comprising the first two transmembrane helices (amino acids (aa) 86–140 of the rPres sequence) exhibits the highest degree of sequence identity across the SLC26

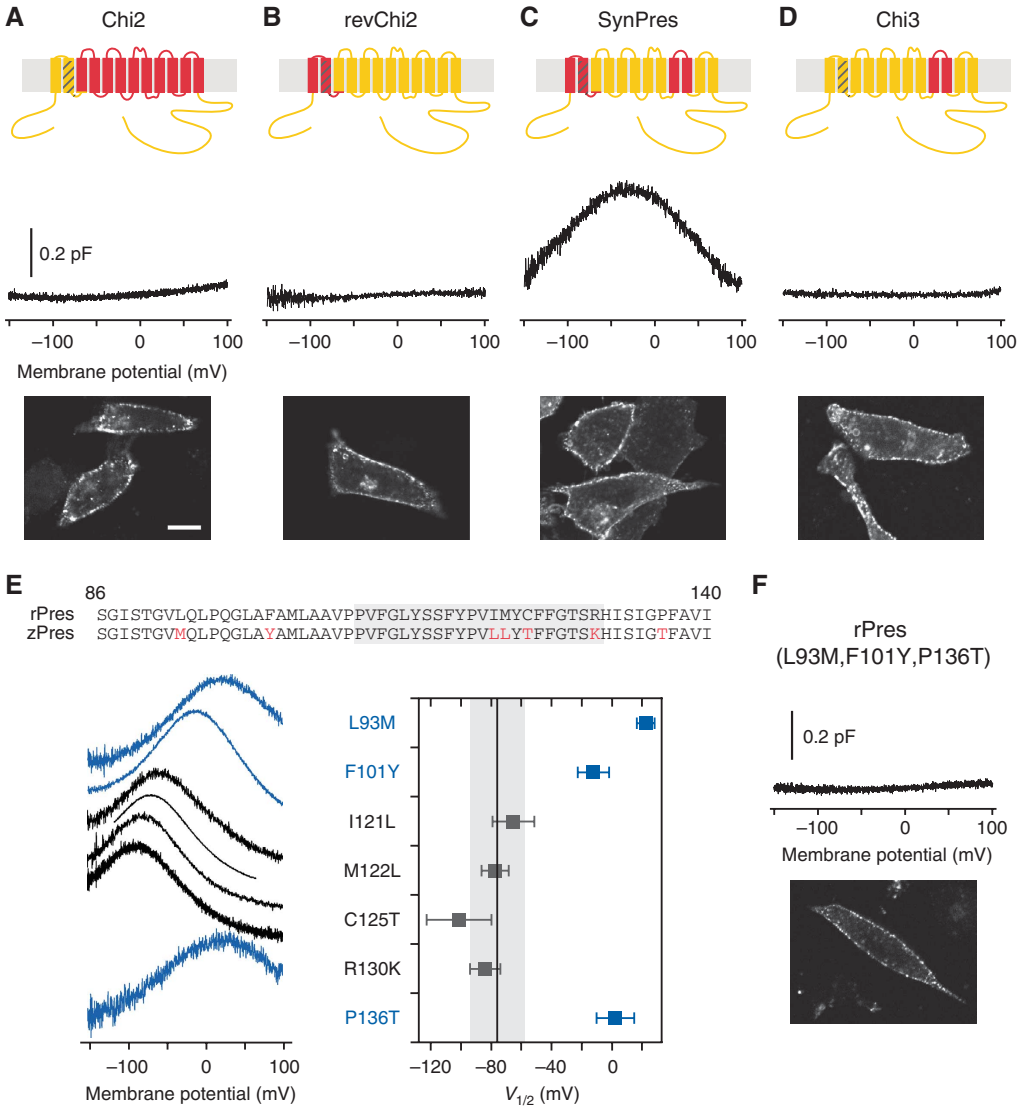

Figure 2 Identification of molecular determinants of NLC and electromotility. (**A**–**D**) The indicated prestin chimeras were expressed in CHO cells as C-terminal GFP fusions and subjected to capacitance measurements (middle panel, NLC traces representative for 5–9 cells with each chimera). All constructs were properly targeted to the plasma membrane as shown by confocal images from representative CHO cells (lower panels; scale bar, 10 μm). Note that NLC was only reconstituted into the zPres background in SynPres, where both domains aa 86–140 (revChi2) and aa 381–438 (Chi3) were combined. (**E**) Sequence alignment of the region exchanged in Chi2 (indexing according to rPres sequence). Non-conserved amino acids are shown in red, the SLC26 signature is boxed. Each of the non-conserved residues in rPres was individually mutated to the respective zPres residue. NLC traces are representative for the indicated mutants, the respective values for $V_{1/2}$ (mean ± s.d.) are given on the right. Solid line and shaded voltage range represent $V_{1/2}$ ± s.d. obtained for rPres ($n = 5$–10 cells for each mutant; for details, see Supplementary Table 1). (**F**) NLC is completely abolished in the triple mutant L93M/F101Y/P136T, although the protein is robustly targeted to the plasma membrane. P136T and the triple mutant were generated in the Chi1 background, because the equivalent mutants in rPres were not delivered to the plasma membrane.

transporter family and includes the highly conserved 'SLC26 transporters signature motif' (residues 109–130; Prosite PS01130; Mount and Romero, 2004). When we replaced this segment in Chi1 with the respective zPres sequence (chimera termed Chi2), NLC was completely abolished (Figure 2A), suggesting that this domain may contain determinants essential for rPres function. Sequence comparison between rPres and zPres showed that only seven amino acids are exchanged within this region, most of them being conservative substitutions (Figure 2E). We next replaced each of these residues in rPres individually by the respective amino acid of zPres and measured the electromotility-related NLC. As shown in Figure 2E, replacement of each of the four positions within the signature motif (I121L, M122L, C124T, R130K) did not substantially affect NLC, while mutating each of the three remaining amino acid exchanges (L93M, F101Y, P136T) shifted NLC towards depolarized potentials by >60 mV (for values of $V_{1/2}$ and α, see Supplementary Table S1). Combining all three mutations completely abolished NLC (Figure 2F), indicating that these three exchanges can fully account for the non-NLC phenotype observed with Chi2 (Figure 2A).

Despite its significance, however, the N-terminal end of the core region is not an exclusive determinant of electromotility

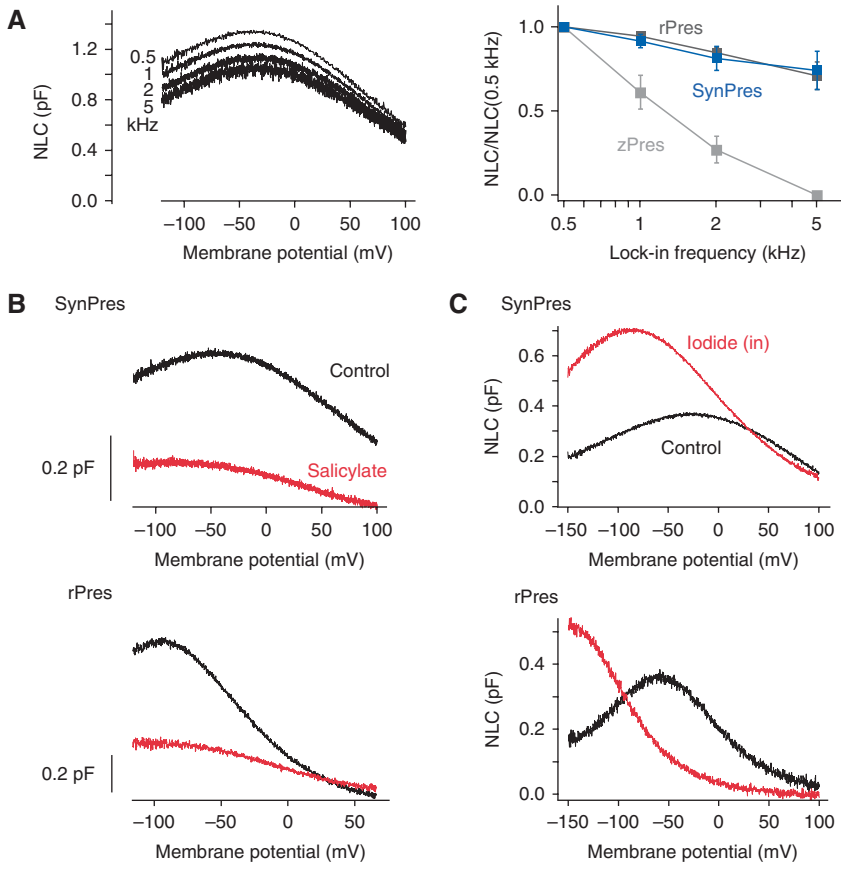

Figure 3 Functional characterization of SynPres. (**A**) Frequency dependence of NLC in SynPres. (Left panel) NLC measured from a CHO cell expressing SynPres with lock-in stimulus sinusoids of 0.5, 1, 2, and 5 kHz. (Right panel) Average NLC amplitudes ($NLC_{max} \pm$ s.d.) normalized to NLC_{max} at 0.5 kHz from cells expressing either rPres ($n = 5$) or SynPres ($n = 8$). Note that frequency dependence of SynPres is identical to rPres; in contrast, zPres shows some NLC only at low frequency stimuli, which rapidly declines to zero towards higher frequencies (zPres data from Albert *et al*, 2007). (**B**) NLC of SynPres and rPres is blocked by salicylate. Traces are representative recordings from the same cell before and during application of 10 mM salicylate added to the extracellular solution. Intracellular solution contained 160 mM Cl^-. (**C**) Intracellular iodide potentiates NLC of both SynPres and rPres and shifts voltage dependence to hyperpolarized potentials. Cells were first patched with a pipette solution containing 160 mM Cl^- as the only anion and subsequently repatched with a pipette solution with 16 mM I^- and 144 mM Cl^- as the intracellular anions.

as revealed by construct revChi2 that placed this segment of rPres into the zPres background. As illustrated by Figure 2B, this domain swapping failed to confer NLC onto zPres and, thus, indicated that the mammalian-specific residues within this region, although necessary, are not sufficient for generation of electromotility-associated NLC. We, therefore, designed a series of additional chimeras where various segments of the rPres core region were successively added onto revChi2. These efforts finally identified another segment comprising putative transmembrane domains 9 and 10 (aa 381–438 in the rPres sequence; Figure 2C; Supplementary Figure S1). On its own, this region was also not sufficient to introduce fast NLC into zPres (Chi3; Figure 2D). However, in combination with the N-terminal segment around transmembrane domains 1 and 2, it generated robust NLC (Figure 2C). This chimera, that we termed SynPres, produced NLC sharing all hallmarks of mammalian prestin, albeit the values for $V_{1/2}$ and α were slightly different ($V_{1/2}$ and α of -22 ± 16 and 69 ± 12 mV, $n = 26$ CHO cells): (i) NLC occurred at high frequencies in contrast to the slow charge movement observed with non-mammalian prestin (Figure 3A; cf. Albert *et al*, 2007); (ii) NLC was blocked by salicylate, an inhibitor of OHC electromotility (Figure 3B); and (iii) NLC displayed the same dependence on intracellular monovalent anions as rPres. Thus, NLC was potentiated by millimolar intracellular iodide (Figure 3C; cf. Oliver *et al*, 2001), and was abolished by the removal of intracellular Cl^- (Figure 7C).

Generation of fast electromotility by SynPres

Next, we probed SynPres for its capability to translate NLC into actual electromotility. Since electromotility induced by recombinant prestin turned out to be difficult to detect in conventional heterologous expression systems, we over-expressed SynPres and rPres in OHCs from prestin knockout mice (Pres−/−; Cheatham *et al*, 2007) via an AAV viral vector (Xia *et al*, 2008; Reisinger *et al*, 2011). Hair cells transduced with rPres or SynPres were whole-cell voltage-clamped, filled with the fluorescent dye Alexa488 via the patch pipette and subjected to sinusoidal voltage stimuli (300 Hz; amplitude ± 40 mV). Cell movement was monitored as changes in fluorescence projected onto a photodiode through a slit aperture positioned across the free basal pole of the OHC (Figure 4A, inset; for details see Materials and methods). While electromotility was completely absent in OHCs from prestin null mice, expression of both SynPres and rPres induced electromotile activity in infected OHCs

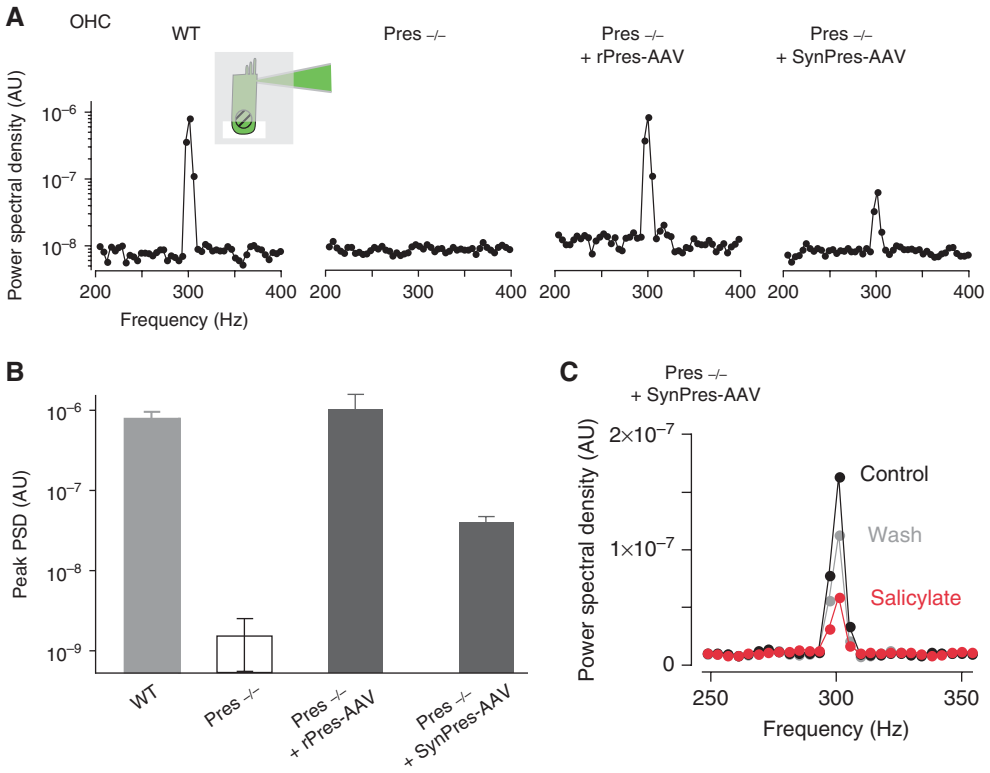

Figure 4 SynPres is an electromotility motor. (**A**) Representative evoked motility recordings from individual OHCs. Longitudinal movements induced by voltage changes were recorded from OHCs in organotypic cultures of the organ of Corti from wild-type mice, from prestin knockout (Pres−/−) mice, or from (Pres−/−) OHCs infected with AAV viral vectors encoding either rPres or SynPres. Cells were filled with Alexa488 through the pipette and length changes were detected as changes in fluorescence projected onto a photodiode through a rectangular aperture positioned across the basal end of the hair cell (inset). Motility was recorded in response to 300 Hz sinusoidal voltage commands (peak-to-peak amplitude 80 mV, holding potential −20 mV) and quantified as the power spectral density of fluorescence intensity. (**B**) Average electromotility measured as peak power spectral density (PSD) at 300 Hz (±s.e.m.) from Pres+/+ OHCs, Pres−/− OHCs, and Pres−/− OHCs expressing either rPres or SynPres ($n = 18$, 13, 9, and 6 cells, respectively). Data are shown with noise floor subtracted. (**C**) Extracellular application of salicylate (10 mM) reversibly inhibited evoked motility in OHCs expressing SynPres.

(Figure 4A and B). Electromotility recorded from SynPres-transduced OHCs was reversibly inhibited by salicylate (Figure 4C). The response amplitude of SynPres was markedly smaller than that observed with rPres (or in wild-type OHCs), most likely as a consequence of the considerably lower expression level of SynPres (estimated from NLC amplitudes; Supplementary Figure S2) and the less steep voltage dependence.

Together, these experiments identified two structural domains in the prestin core (termed NLC-domains 1 and 2 hereafter) that are both necessary and sufficient for the generation of electromotility and NLC by an SLC26 transporter. Although distantly located in the primary sequence of prestin, these two domains jointly convert the non-mammalian zPres into a membrane motor with characteristics very similar to those observed with mammalian prestin.

SynPres features both electromotility and transport activity

Subsequent analysis showed that, despite the newly acquired NLC and electromotility, SynPres retained electrogenic anion transport activity, the hallmark of non-mammalian SLC26A5. When the divalent oxalate (10 mM) was included in the patch pipette (Schaechinger and Oliver, 2007), SynPres produced robust inward currents that were reversibly inhibited by salicylate (Figure 5A). At this steep outward concentration gradient for oxalate and a 10:1 inward gradient for Cl^-, the transport current, defined as the salicylate-sensitive whole-cell current, reversed at around 100 mV (Figure 5B), consistent with the same 1:1 stoichiometric antiport of oxalate versus chloride previously determined for non-mammalian SLC26A5 (Schaechinger and Oliver, 2007). Thus, the anion transport mechanism of zPres appeared largely unimpaired by the introduction of the NLC-domains 1 and 2.

We probed involvement of both domains in anion transport by a detailed examination of substrate specificity in the chimeras containing one or both NLC-conferring domains from mammalian prestin. To this end, the two known divalent transport substrates, oxalate and sulphate (10 mM each), were applied successively to cells expressing zPres or the chimeras. For zPres, robust net outward currents resulting from stoichiometric exchange of the divalent anion (inward) against chloride (outward) (Schaechinger and Oliver, 2007) were similar with oxalate and sulphate: the ratio of conductances (G(oxalate)/G(sulphate)) was 1.5 (Figure 5C and F), indicating little selectively among both substrates. Strikingly, insertion of NLC-domain 1 into zPres (revChi2) dramatically changed this ratio to 8.9 (Figure 5D and F), indicating pronounced preference for oxalate over sulphate. In SynPres, additionally containing NLC-domain 2 from rPres, the conductance ratio was restored to 1.6 (Figure 5E and F). Thus, both structural domains have substantial impact on ion

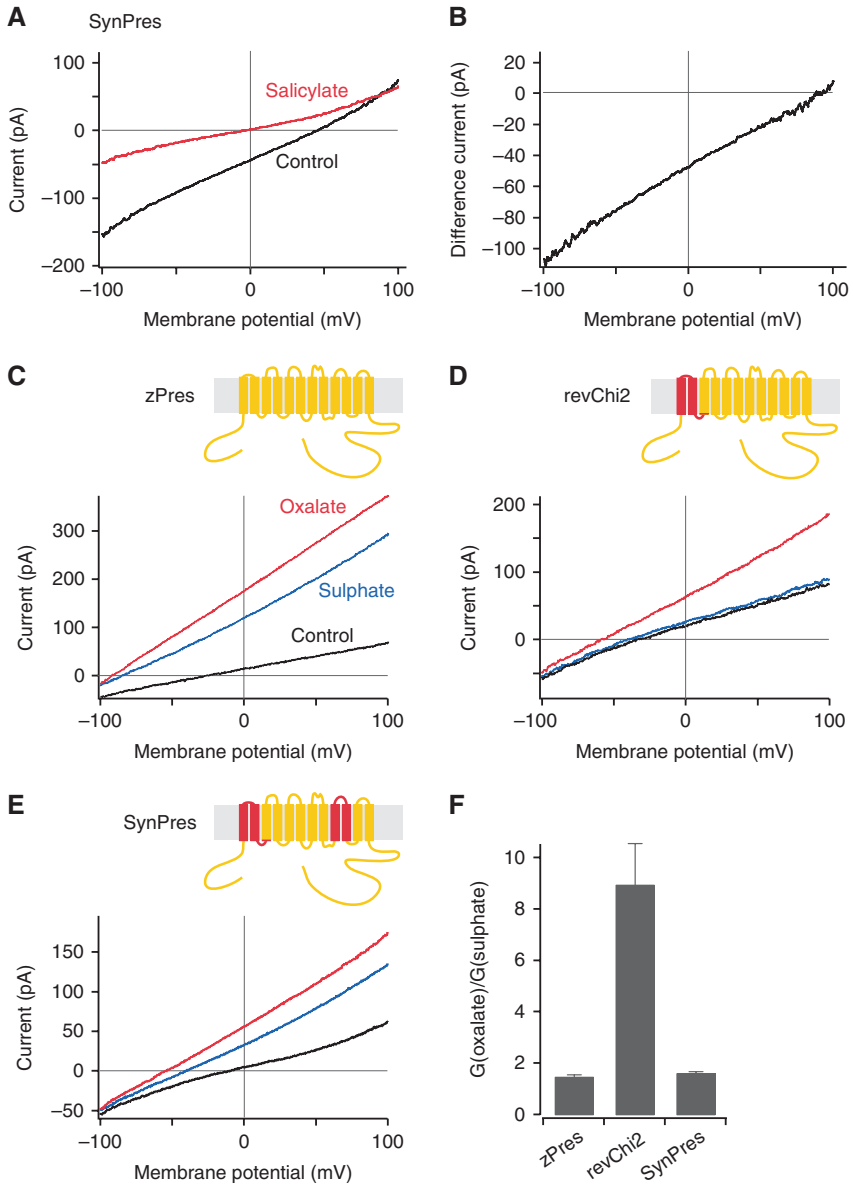

Figure 5 Electrogenic transport of divalent anions by SynPres. (**A**) Transport currents recorded from a SynPres expressing CHO cell in the presence of the divalent substrate oxalate (intracellular solution contained 10 mM oxalate^{2-}, 10 mM Cl^-, and 130 mM aspartate$^-$). Oxalate outward transport is readily identified by the positive reversal potential and the current inhibition by salicylate (10 mM). (**B**) Salicylate-sensitive transport current isolated by subtraction from the data in (**A**). (**C**–**E**) Representative transport currents generated by zPres (**C**), revChi2 (**D**), and SynPres (**E**) in the presence of the divalent transport substrates oxalate (red) or sulphate (blue) applied extracellularly. Whole-cell currents obtained from the same cells in the absence of divalent substrates are shown in black (control). (**F**) Ratios of transport conductance for both substrates obtained from experiments as in (**C**–**E**). Slope conductance at 0 mV was measured after subtraction of background currents. Data are mean (± s.e.m.) of 9 (zPres), 8 (revChi2), and 9 (SynPres) cells.

selectivity of transport and appear to cooperate not only in conferring NLC/electromotility but also in determining substrate selectivity, most likely by establishing an anion-binding site or part of the anion permeation pathway.

Interdependence of electromotility and transport

Notably, in the presence of the divalent transport substrate, both NLC and transport current of SynPres could be recorded simultaneously (Figure 6A). As illustrated in Figure 6B, the amplitudes of the transport current and the NLC were closely correlated across different cells, corroborating their simultaneous generation by SynPres. Given that in SynPres, NLC and consequently electromotility operate while anions permeate through the transport pathway, the finding of common structural determinants immediately raised the question of potential interaction and mechanistic relation of both processes.

With NLC and transport activity occurring simultaneously, SynPres provided a novel experimental approach for analysing such interaction. Thus, we probed for reciprocal interference of NLC and anion transport by measuring NLC in SynPres with anion exchange activity switched either on or off. For this purpose, NLC was measured from the same cells expressing rPres or SynPres before (first whole-cell recording; Figure 7A, inset) and after addition of the transport substrate oxalate (10 mM) to the patch pipette (second whole-cell recording); only the latter configuration promotes

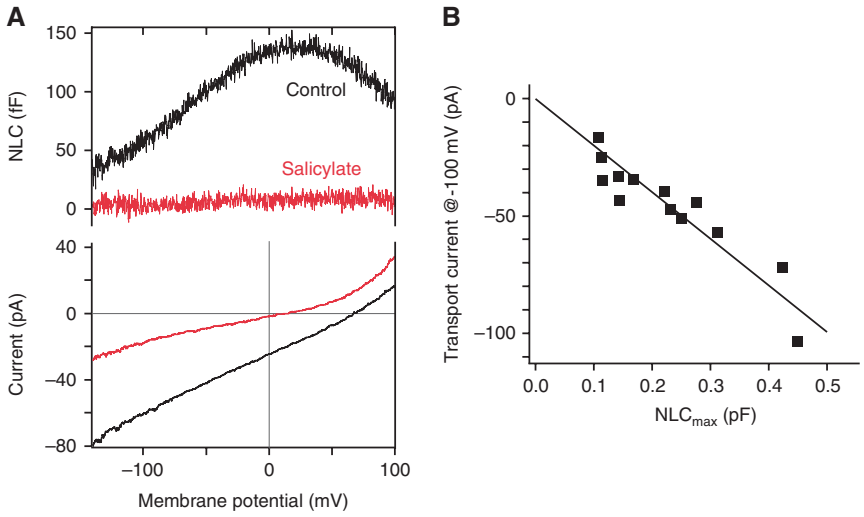

Figure 6 Simultaneous anion transport and NLC in SynPres. (**A**) NLC of SynPres measured during anion transport. NLC and transport current were recorded simultaneously in the presence of intracellular oxalate (recording conditions as in Figure 5A) before and during application of 10 mM salicylate. (**B**) Correlation of NLC and transport current amplitudes obtained from 13 cells as in (**A**). Transport current was determined as the salicylate-sensitive whole-cell current at −100 mV. Solid line represents a linear regression.

Cl^-/oxalate exchange activity that can be monitored as a transport current simultaneous to NLC measurements. This transport mode was the only one possible under the experimental conditions, since Cl^- and oxalate were the only monovalent and divalent transport substrates present, respectively (cf. Schaechinger and Oliver, 2007).

When anion transport was elicited by intracellular oxalate, the amplitude of the NLC mediated by SynPres increased by 2.14 ± 0.46-fold (mean ± s.d., $N = 8$ cells; Figure 7A and B) compared with the zero transport condition before addition of the divalent (intracellular and extracellular Cl^-, 10 and 160 mM, respectively). In contrast, in mammalian prestin lacking transport activity, addition of intracellular oxalate markedly reduced NLC (to 0.58 ± 0.06 of control, $N = 6$; Figure 7A and B), despite the constant intracellular concentration of Cl^-. A similar reduction of NLC by intracellular oxalate was observed with native prestin in rat OHCs (Supplementary Figure S3). In either case, $V_{1/2}$ was shifted to slightly more positive potentials (by 34.1 ± 11.9 mV and by 5.5 ± 6.6 mV for recombinant SynPres and rPres, respectively; Figure 7A). The enhancement of NLC exclusively in the transport-competent SynPres suggested an influence of anion transport on the generation of NLC.

Subsequent experiments that further investigated the nature of the oxalate-induced increase in NLC amplitude directly demonstrated that inward transport of the monovalent Cl^- was the prerequisite for this striking phenomenon observed with SynPres. These experiments were done in the absence of intracellular Cl^- (substitution by aspartate), which fully abolished NLC (Figure 7C; upper panel), consistent with previous observations on rPres (Oliver *et al*, 2001). Loss of NLC indicated that binding of Cl^- from the intracellular face is required to support NLC in the absence of anion exchange activity. However, robust NLC could be measured with oxalate (10 mM) in the cytoplasm and, at the same time, Cl^- (160 mM) present at the extracellular side of the membrane, which promoted inward transport of the monovalent monitored as the transport current (Figure 7C, middle left panel). When anion transport was switched off by removal of one of the two substrates, either Cl^- from the extracellular milieu or oxalate from the cytoplasm, NLC was no longer recorded (Figure 7C, upper and lower left panels, respectively). Moreover, control experiments with oxalate on both sides of the membrane (160 mM extracellular, 10 mM intracellular) demonstrated that the divalent *per se* was not sufficient to support NLC in SynPres (data not shown). Finally, oxalate (10 mM) added to the cytoplasm failed to trigger NLC in the transport-incompetent rPres both in the absence and in the presence of high concentrations of Cl^- in the extracellular solution (Figure 7C, right panel).

Several observations indicate that the observed potentiation of NLC by anion transport resulted from a genuine interaction of both processes rather than from an accumulation of Cl^- at the intracellular side. First, a two-fold increase was observed even in the presence of 10 mM Cl^- in the intracellular medium (Figure 7A and B). Given the known sensitivity of NLC for intracellular Cl^- (Oliver *et al*, 2001), the cytoplasmic concentration of Cl^- would need to be elevated by > 100 mM to double the NLC amplitude, which seems incompatible with the '[Cl^-] clamp' by the whole-cell patch-clamp and the small transport current. Second, the change of NLC (Figure 7C, middle panel) occurred simultaneous (without any time lag) with the change of the extracellular concentrations monitored by transport current reversal, arguing against a requirement for transport-dependent accumulation of intracellular Cl^-.

In summary, these experiments indicated that generation of the electromotility-related NLC in prestin is tightly linked to anion transport. Specifically, NLC requires (i) monovalent anions such as Cl^- or other anion species (Rybalchenko and Santos-Sacchi, 2008) that (ii) must be translocated to an interaction/binding site within the protein. In SynPres, this translocation may occur from either the extracellular (through divalent/chloride electrogenic antiport) or the intracellular side of the membrane (independent of divalent-triggered transport), while in the transport-deprived rPres

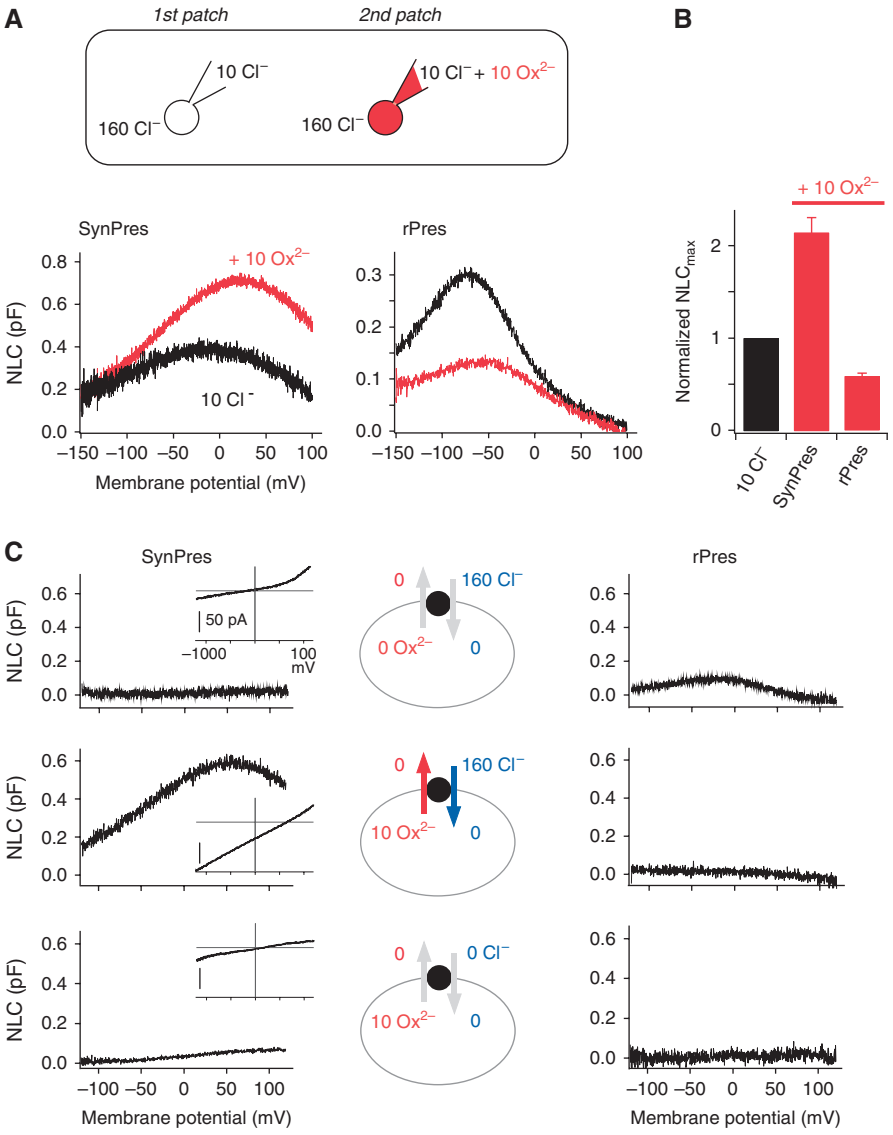

Figure 7 Functional interaction of electromotility-related NLC and anion permeation. (**A**) Addition of intracellular oxalate increased NLC in SynPres but impaired NLC in rPres. NLC from cells expressing SynPres (left panel) or rPres (right panel) measured in the absence and subsequently in the presence of the divalent transport substrate oxalate. Inset: The cell was patched twice with different intracellular solutions containing either 10 mM Cl^- (black) or 10 mM Cl^- plus 10 mM oxalate^{2-} (red); extracellular solution contained 160 mM Cl^-. (**B**) Mean NLC amplitudes (± s.e.m.) recorded in experiments as in (**A**). NLC_{max} was normalized to NLC_{max} in the absence of oxalate (intracellular 10 mM Cl^- only) for each cell. ($n = 8$ and 6 cells for SynPres and rPres, respectively). (**C**) NLC recordings from SynPres (left panels) and rPres (right panels) under the various ionic conditions indicated in the middle panels: removal of intracellular Cl^- (substitution by aspartate, upper lane), addition of intracellular oxalate (10 mM, middle lane), and additional removal of extracellular Cl^- (lower lane). Insets for SynPres (left panels) show corresponding transport current measurements from the same cells, confirming substantial transport activity only in the presence of intracellular oxalate and extracellular Cl^-. Data shown are representative examples from 4–12 experiments for each condition. Note that substantial NLC was only recorded under conditions promoting inward transport of Cl^-. Residual NLC obtained with 10 mM intracellular oxalate and 0 mM extracellular Cl^- (lower left panel; 12 ± 3% of NLC obtained at 160 mM extracellular Cl^-) can be attributed to residual transport as indicated by the positive reversal potential (inset).

NLC can only be triggered by monovalents from the intracellular milieu. Suppression of NLC by oxalate in rPres indicates that divalents can still bind to the defective transporter, possibly competing binding of the NLC-promoting monovalent anion.

Discussion

The central findings of the present work are the identification of structural domains in the transmembrane core of prestin that are both necessary and sufficient for fast electromotility and the observation that transport/translocation of monovalent anions is a prerequisite for generation of NLC and hence electromotility of mammalian prestin.

Structural determinants of NLC and electromotility

Fast electromotility of OHCs is generated by prestin proteins densely packed in the basolateral membrane and operating as piezoelectric-like elements that convert changes in membrane potential into length changes (Iwasa, 2001; Ludwig

et al, 2001) and thereby produce the mechanical force crucial for active cochlear amplification (Ashmore, 2008; Dallos, 2008; Dallos *et al*, 2008). Conversion between electrical and mechanical energy by prestin is fully reciprocal (Iwasa, 2001; Ludwig *et al*, 2001) and requires intracellular anions as an extrinsic factor (Oliver *et al*, 2001; Rybalchenko and Santos-Sacchi, 2008). How anions initiate the coupling of mechanical and electrical action, however, has remained elusive, in particular as structural information on the functionally important core region of prestin and of other SLC26 transporters is largely missing. Despite some initial work towards respective structure–function analyses (Oliver *et al*, 2001; Navaratnam *et al*, 2005; Rajagopalan *et al*, 2006; Bai *et al*, 2009; McGuire *et al*, 2010), no data are yet available that firmly link distinct protein domains of prestin to particular functions, such as voltage-sensing or motility-generating transitions.

Using domain swapping between rPres and zPres together with measurements of transport currents and capacitance we identified structural elements required for piezoelectricity: two distinct stretches in the rPres polypeptide, one comprising transmembrane domains 1 and 2 and the adjacent linker (aa 93–136; NLC-domain 1), the other consisting of putative transmembrane domains 9 and 10 (aa 381–438; NLC-domain 2). Despite the strikingly large distance in primary sequence, these two domains closely cooperate in function and effectively combine to endow the exclusive transporter zPres with NLC and fast electromotility (Figures 2–4). Moreover, function of SynPres, the 'gain-of-function' rPres–zPres chimera, strongly suggests that the NLC-domains are placed right at the interface between electromotility and anion transport and that they may even form part of the anion permeation pathway. Such a structural view is supported by the fact that monovalent anions must be translocated into the protein before NLC/electromotility can occur (Figure 7). In addition, it is noteworthy that the NLC-domain 1 coincides with the region of highest sequence conservation across the large family of SLC26-related SulP transporters and includes the SLC26A signature motif (PS01130) implicated in transport function (Leves *et al*, 2008). Individual residues within NLC-domain 1 that were found to be critical for electromotility and NLC (L93, F101, and P136) are essentially conserved among prestins from all mammalian clades (Supplementary Figure S4), which share electromotility and NLC (Okoruwa *et al*, 2008; Tan *et al*, 2011). Vice versa, across all non-mammalian SLC26A5 sequences, these residues are also highly conserved but distinct from the mammalian forms, indicating a critical role of these residues for electromotility in mammalian and for transport in non-mammalian prestins. This observation further suggests that these amino acid exchanges were key events in the evolutionary conversion from a transporter to a piezoelectric protein and strongly supports the important role of NLC-domain 1 for prestin function.

It should be noted that additional regions of prestin are probably involved in shaping the exact functional properties of mammalian prestin, since voltage sensitivity of SynPres differs substantially from native mammalian prestin.

The finding of two discrete domains closely cooperating in driving translocation of ions is reminiscent of two bacterial transporters for which high-resolution structural data are available, the Na^+/H^+ antiporter NhaA (Hunte *et al*, 2005) and the Cl^-/H^+ antiporter Ec-ClC (Dutzler *et al*, 2002, 2003; Accardi and Miller, 2004; Miller, 2006). In either case, the ion pathway is built from α-helical segments (conventional and discontinuous) separated in the respective primary sequence by seven helical domains (helices IV and XI in NhaA or segments E/F and M/N in Ec-ClC) and offers binding site(s) for the respective substrates. In particular, in NhaA, these ion-binding sites are right in the middle of the membrane; binding of the charged substrates to these sites are thought to induce movements of the helical domains, which in turn promote substrate translocation according to an alternating-access mechanism (Hunte *et al*, 2005).

Molecular model for generation of NLC and electromotility

Based on the structural similarities with NhaA, an alternating-access mechanism may be envisaged as the structural and functional principle behind the coupling of transport and NLC/electromotility observed for rPres and SynPres (Figure 7). As a straightforward explanation for changes in NLC amplitude, the transport process may determine the occupancy of a structural conformation ('active state') that enables the voltage-fuelled rapid elongation/contraction transition generating NLC and fast electromotility. According to our results, this active state corresponds to a conformation in which a monovalent anion occupies a binding site within prestin's permeation pathway. In SynPres, this binding site is reached either from the cytoplasm or from the extracellular side of the membrane (through an alternating-access cycle driven by divalent anions such as oxalate); in rPres, where the transport cycle is constitutively blocked (most likely by amino acid exchanges in the mammalian NLC-domains compared with their non-mammalian counterparts), the monovalent anions can reach the intramolecular binding site from the cytoplasm only (Figure 7).

Figure 8 illustrates an alternating-access model that can account for the observed behaviour of both rPres and SynPres; in fact, it displays some similarity with a scheme proposed by Muallem and Ashmore (2006). Stoichiometric antiport (as observed with SynPres) is realized by transitions between the two major conformations with the substrate binding site facing either the cytosol (E_i) or the extracellular space (E_o); transitions between E_i and E_o only occur upon substrate binding. The distribution between the various states depends on transport rates and substrate concentrations. In this model, the 'active state' that exclusively undergoes the voltage-driven piezoelectric transition is assigned to the Cl-bound state E_oCl (highlighted in yellow; Figure 8), consistent with the requirement of Cl^- binding for generation of NLC (Figure 7C; Oliver *et al*, 2001, 2006).

Qualitative inspection of the model readily reveals that in SynPres, induction of transport by addition of the divalent substrate leads to redistribution between states, including an altered occupancy of the active state and thus altered NLC amplitude. Of note, transitions within the transport cycle may be much slower than the ultrafast conformational changes that generate force and NLC without limiting the kinetics of the latter, which are voltage-driven conformational changes between sub-states of the 'active state' as depicted in Figure 8. Specifically, binding of intracellular oxalate to E_i drives additional prestin molecules into the active state, thus increasing NLC consistent with experimental findings

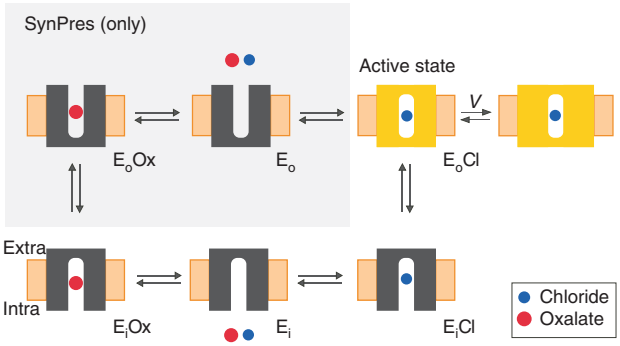

Figure 8 Alternating-access model for operation of rPres and SynPres. Anion transport (in SynPres only) occurs through transitions between two major conformations, with the anion-binding site exposed either to the cytosol (E_i) or to the extracellular side (E_o). Binding and dissociation of Cl^- (blue) and oxalate (red) occurs from both major states; transitions between the E_i and E_o conformations require substrate binding. SynPres may adopt all states shown, while for rPres only states in the non-shaded area are accessible. Specifically, binding and unbinding of Cl^- to and from E_o is impossible in rPres, as symbolized by the external barrier in the permeation pathway. NLC is generated exclusively by prestin molecules residing in the Cl^--bound E_oCl state ('active state'; yellow). More precisely, NLC arises from fast voltage-dependent transitions between the states highlighted in yellow, for simplicity lumped into E_oCl (V, membrane potential). Note, that the difference in extension between NLC-generating states is merely meant to symbolize area motor activity and that assignment of extended versus compact state is chosen arbitrarily.

(Figure 7A). The reason for this is the increase in overall rates towards the outward-facing conformations and the rapid unidirectional transition from E_oOx to the active state (in the absence of extracellular divalent substrate). This effect is particularly pronounced if the transition between E_iOx and E_oOx is faster than the transition between E_iCl and active state. A detailed quantitative analysis of the model confirms this conclusion (see Supplementary Figure S5).

Moreover, the model readily predicts the suppressive effect of intracellular oxalate on NLC generated by rPres: because NLC is completely independent of extracellular Cl^- (Oliver *et al*, 2001), dissociation from and binding of Cl^- to the outward-facing conformation must be impossible or greatly disfavoured (shaded in Figure 8). This is also consistent with the lack of transport activity in rPres (Schaechinger and Oliver, 2007; Tan *et al*, 2011). Hence, when binding of intracellular oxalate increases occupancy of E_iOx, occupancy of E_oCl and consequently NLC must decrease, consistent with the experimental findings shown in Figure 7A and B.

Furthermore, results obtained in the absence of intracellular Cl^- (Figure 7C) are in good agreement with the predictions derived from the alternating-access transport model. Briefly, loss of NLC upon removal of intracellular Cl^- is readily explained by accumulation of prestin in the E_i state that cannot promote NLC. Addition of intracellular oxalate leads to suppression of NLC in rPres via additional trapping of prestin molecules in the E_iOx state, whereas in SynPres, intracellular oxalate allows for divalent/chloride antiport, which runs exclusively clockwise in the absence of extracellular oxalate and shuttles prestin molecules from E_i towards the E_o conformations. As a consequence, occupancy of the active state must increase, in agreement with the observed increase in NLC amplitude. Removal of extracellular Cl^- interrupts transport since the transition from Eo to the active state becomes zero. As this prevents refilling of the active state, NLC should be abolished as indeed observed experimentally.

Finally, the results presented in Figure 7C also exclude an alternative allosteric mechanism that was suggested previously for various intracellular anions (Rybalchenko and Santos-Sacchi, 2008), namely potentiation of NLC by intracellular oxalate through binding to a distinct site. Thus, intracellular oxalate promoted NLC only in the presence of extracellular Cl^-, but not when extracellular Cl^- was removed (Figure 7C) or when only oxalate was present at both sides of the membrane.

In summary, the dependence of NLC on transport substrates in both SynPres and mammalian prestin is fully consistent with a model in which the NLC-generating transition is embedded within an alternating-access transport cycle. Notably, the presented model does not make any assumption about the nature of the NLC-generating transition; NLC may derive from shuttling of Cl^- through the electric field (Oliver *et al*, 2001) or from movement of an intrinsic voltage sensor (Bai *et al*, 2009) or a combination of both.

Materials and methods

Molecular biology

cDNAs coding for native, mutant, or chimeric prestin proteins were derived from *Rattus norvegicus* and *Danio rerio* prestin cDNAs (GenBank accession No. NM_030840 and BC054604.1, respectively) by standard molecular biology techniques and cloned into pEGFP-N1 (Clontech) (rPres, Chi1, Chi2, revChi2, SynPres) or pEGFP-N3 (zPres, Chi3), yielding C-terminal GFP fusion constructs. All constructs were verified by sequencing. For viral infection of OHCs, rPres and SynPres were subcloned into the viral vector AAV-HBA-EWB (Kugler *et al*, 2007).

Electrophysiology

cDNAs containing pEGFP plasmids were transfected into CHO cells using JetPEI transfection reagent (Polyplus, Illkirch, France). For electrophysiological experiments (24–48 h after transfection), cells with unequivocal and comparable membrane fluorescence were selected. Whole-cell patch-clamp recordings were carried out at room temperature (20–22°C) with EPC10 amplifiers (Heka, Lambrecht, Germany) controlled by Patchmaster software (Heka).

NLC. Whole-cell membrane capacitance (C_M) was recorded using the sine + DC software lock-in function of Patchmaster. Frequency of stimulus sinusoids was 2 kHz unless indicated otherwise. Voltage-dependent NLC was assessed by recording C_M during voltage ramps (slope +0.2 to +0.56 V/s) as described previously (Oliver and Fakler, 1999; Schaechinger and Oliver, 2007) and plotted as a function of membrane potential (V_M). Traces shown usually represent averages from 2 to 10 individual capacitance traces.

NLC was quantified by fitting the derivative of a first-order Boltzmann function to the $C_M(V_M)$ traces,

$$C_M(V_M) = C_{lin} + \frac{Q_{max}}{\alpha e^{\frac{V-V_{1/2}}{\alpha}}\left(1+e^{-\frac{V-V_{1/2}}{\alpha}}\right)^2} \quad (1)$$

where C_{lin} is linear membrane capacitance, V_M is membrane potential, Q_{max} is maximum voltage-sensor charge moved through the membrane electric field, $V_{1/2}$ is voltage at half-maximal charge transfer, and α is the slope factor of the voltage dependence. The amplitude of NLC was quantified as peak NLC, $NLC_{max} = C_M(V_{1/2}) - C_{lin}$. As a measure of expression level, NLC was normalized to linear membrane capacitance, which is proportional to plasma membrane area: $NLC_{rel} = NLC_{max}/C_{lin}$.

Transport. Electrogenic anion transport was measured as the ionic transport current in response to command voltage ramps (−100 to

+100 mV; 0.5 or 1 V/s) as described previously (Schaechinger and Oliver, 2007).

Solutions. For NLC recordings, patch pipettes were filled with intracellular solution containing 160 mM CsCl. For experiments with intracellular iodide, 15 mM CsI was substituted for an equal concentration of CsCl. For transport or combined transport and NLC measurements, intracellular solution was (in mM) 10 CsCl, 10 oxalate, 130 K-aspartate, pH 7.3 (KOH), or 10 CsCl, 150 K-aspartate. For measurements with nominally Cl^--free conditions, pipettes were tip-filled with solution of either 160 mM K-aspartate or 150 mM K-aspartate and 10 mM oxalate. Pipettes were back-filled with Cl^--containing solutions to ensure stable electrode offset. All pipette solutions additionally contained 1 mM Hepes, 1 mM K_2EGTA, and pH was adjusted to 7.3 with KOH. Unless specified otherwise, extracellular solution was (in mM): 144 NaCl, 5.8 KCl, 1.3 $CaCl_2$, 0.9 $MgCl_2$, 10 Hepes, 0.7 Na_2HPO_4, and 5.6 glucose, pH 7.4 (NaOH). For inhibition of anion transport and NLC, 10 mM sodium salicylate was added. For exchange of extracellular Cl^-, solutions were simplified to contain either (in mM) 160 KCl and 5 Hepes, or 160 K-aspartate and 5 mM Hepes, pH 7.4 with KOH. For extracellular application of divalent transport substrates solutions contained either 10 mM Na_2-oxalate or Na_2SO_4 and (in mM) 1 NaCl, 149 Na-aspartate, 2 Mg-gluconate, 10 Hepes, pH 7.4 with NaOH. An agarose bridge was used as the bath electrode whenever extracellular anions were exchanged.

Organotypic culture and viral transduction

Organotypic cultures of organs of Corti from mice at days 6–7 after birth were prepared and cultured as reported previously (Oliver *et al*, 1997). Mice were either homozygous prestin null mice (Cheatham *et al*, 2007) (Pres −/−) or control C57BL/6 mice (wt). AAV vectors of the hybrid serotype 1/2 were constructed essentially as described (Kugler *et al*, 2007; Reisinger *et al*, 2011). Expression was driven by the β-actin promoter. Recombinant AAVs were purified by iodixanol gradient centrifugation and FPLC on heparin affinity columns. Vectors were dialysed against PBS and stored at −80°C in single use aliquots. Purity >99% was confirmed by SDS–PAGE and silver staining, genome titres were quantified by real-time PCR.

Cultures from Pres−/− mice were infected with AAV vectors encoding either rPres or SynPres (2 μl per 0.3 ml well) in serum-free medium at 1 day *in vitro*. Measurements were done after 6–8 days *in vitro* (5–7 days after infection), when prestin expression levels had reached saturation as determined from NLC recordings (unpublished results).

Electromotility

For NLC and electromotility measurements, OHCs were whole-cell patch-clamped, using standard extracellular solution (see above) and an intracellular solution composed of (in mM): 150 NaCl, 2.5 Na_2ATP, 2 HEPES, 1 K_2EGTA, 0.1 AlexaFluor488 hydrazide (Invitrogen), pH 7.3 (KOH), osmolality 290 mosm/kg. This solution was found to minimize endogenous ionic currents and to support robust electromotile responses. The patch pipette was positioned with an MM3A-LS piezoelectric manipulator (Kleindiek Nanotechnik, Reutlingen, Germany) to exclude vibrational artifacts.

OHCs oriented with their longitudinal axis parallel to the coverslip were patch-clamped with the pipette sealed onto the lateral membrane close to the cuticular plate after gently removing neighbouring supporting cells, allowing movement of the basal cell pole. Fluorescence from Alexa488-filled OHCs was obtained with widefield fluorescence optics and a conventional EGFP filter set. Fluorescence from the basal pole of the cell was selectively projected onto a photodiode through a rectangular aperture positioned across the basal OHC pole (see Figure 4A, inset) by means of a Viewfinder photometry device (Till Photonics, Gräfelfing, Germany). OHC length changes evoked by sinusoidal voltage commands (20 mV ± 40 mV, 300 Hz), resulted in changes of fluorescence intensity. These fluorescence changes recorded as the uncalibrated photodiode output were used as the measure for electromotility. Electromotility was then quantified by calculating power spectra from raw fluorescence data using IgorPro software (IgorPro; Wavemetrics, Lake Oswego) and by analysing power spectral density at the stimulus frequency (300 Hz).

Motility recordings from virus-infected OHCs were restricted to those cells displaying a clearly discernable NLC that was inhibited by salicylate (10 mM), indicating successful expression of exogenous prestin construct. Such salicylate-sensitive NLC was never detected in non-infected Pres−/− OHCs.

Confocal microscopy

Live CHO cells transfected with GFP-fused prestin constructs were imaged with a Zeiss LSM710 confocal microscope with GFP excitation at 488 nm.

Supplementary data

Supplementary data are available at *The EMBO Journal* Online (http://www.embojournal.org).

Acknowledgements

We thank Anna Bulankina for initial characterization of the AAV vector and for sharing experimental protocols, Mary-Ann Cheatham and Peter Dallos for providing prestin null mice and Olga Ebers for expert technical assistance.

Author contributions: TJS and DO designed and performed the experiments and analysed the data; DG designed and performed the experiments; CRH generated the mathematical model; SK and TM developed and generated viral vectors; DO and BF conceived the study and wrote the manuscript.

Conflict of interest

The authors declare that they have no conflict of interest.

References

Accardi A, Miller C (2004) Secondary active transport mediated by a prokaryotic homologue of ClC Cl- channels. *Nature* **427:** 803–807

Albert JT, Winter H, Schaechinger TJ, Weber T, Wang X, He DZZ, Hendrich O, Geisler H-S, Zimmermann U, Oelmann K, Knipper M, Gopfert MC, Oliver D (2007) Voltage-sensitive prestin orthologue expressed in zebrafish hair cells. *J Physiol* **580:** 451–461

Ashmore J (2008) Cochlear outer hair cell motility. *Physiol Rev* **88:** 173–210

Ashmore JF (1987) A fast motile response in guinea-pig outer hair cells: the cellular basis of the cochlear amplifier. *J Physiol* **388:** 323–347

Bai J-P, Surguchev A, Montoya S, Aronson PS, Santos-Sacchi J, Navaratnam D (2009) Prestin's anion transport and voltage-sensing capabilities are independent. *Biophys J* **96:** 3179–3186

Bezanilla F (2008) How membrane proteins sense voltage. *Nat Rev Mol Cell Biol* **9:** 323–332

Brownell WE, Bader CR, Bertrand D, de Ribaupierre Y (1985) Evoked mechanical responses of isolated cochlear outer hair cells. *Science* **227:** 194–196

Cheatham MA, Zheng J, Huynh KH, Du GG, Edge RM, Anderson CT, Zuo J, Ryan AF, Dallos P (2007) Evaluation of an independent prestin mouse model derived from the 129S1 strain. *Audiol Neurootol* **12:** 378–390

Dallos P (2008) Cochlear amplification, outer hair cells and prestin. *Curr Opin Neurobiol* **18:** 370–376

Dallos P, Fakler B (2002) Prestin, a new type of motor protein. *Nat Rev Mol Cell Biol* **3:** 104–111

Dallos P, Wu X, Cheatham MA, Gao J, Zheng J, Anderson CT, Jia S, Wang X, Cheng WHY, Sengupta S, He DZZ, Zuo J (2008) Prestin-based outer hair cell motility is necessary for mammalian cochlear amplification. *Neuron* **58:** 333–339

Dutzler R, Campbell EB, Cadene M, Chait BT, MacKinnon R (2002) X-ray structure of a ClC chloride channel at 3.0 A reveals the molecular basis of anion selectivity. *Nature* **415:** 287–294

Dutzler R, Campbell EB, MacKinnon R (2003) Gating the selectivity filter in ClC chloride channels. *Science* **300:** 108–112

Franchini LF, Elgoyhen AB (2006) Adaptive evolution in mammalian proteins involved in cochlear outer hair cell electromotility. *Mol Phylogenet Evol* **41:** 622–635

Frank G, Hemmert W, Gummer AW (1999) Limiting dynamics of high-frequency electromechanical transduction of outer hair cells. *Proc Natl Acad Sci USA* **96:** 4420–4425

Hudspeth AJ (2008) Making an effort to listen: mechanical amplification in the ear. *Neuron* **59:** 530–545

Hunte C, Screpanti E, Venturi M, Rimon A, Padan E, Michel H (2005) Structure of a Na+/H+ antiporter and insights into mechanism of action and regulation by pH. *Nature* **435:** 1197–1202

Iwasa KH (2001) A two-state piezoelectric model for outer hair cell motility. *Biophys J* **81:** 2495–2506

Kugler S, Hahnewald R, Garrido M, Reiss J (2007) Long-term rescue of a lethal inherited disease by adeno-associated virus-mediated gene transfer in a mouse model of molybdenum-cofactor deficiency. *Am J Hum Genet* **80:** 291–297

Leves FP, Tierney ML, Howitt SM (2008) Polar residues in a conserved motif spanning helices 1 and 2 are functionally important in the SulP transporter family. *Int J Biochem Cell Biol* **40:** 2596–2605

Ludwig J, Oliver D, Frank G, Klocker N, Gummer AW, Fakler B (2001) Reciprocal electromechanical properties of rat prestin: the motor molecule from rat outer hair cells. *Proc Natl Acad Sci USA* **98:** 4178–4183

McGuire RM, Liu H, Pereira FA, Raphael RM (2010) Cysteine mutagenesis reveals transmembrane residues associated with charge translocation in prestin. *J Biol Chem* **285:** 3103–3113

Miller C (2006) ClC chloride channels viewed through a transporter lens. *Nature* **440:** 484–489

Mount DB, Romero MF (2004) The SLC26 gene family of multifunctional anion exchangers. *Pflugers Arch* **447:** 710–721

Muallem D, Ashmore J (2006) An anion antiporter model of prestin, the outer hair cell motor protein. *Biophys J* **90:** 4035–4045

Navaratnam D, Bai J-P, Samaranayake H, Santos-Sacchi J (2005) N-terminal-mediated homomultimerization of prestin, the outer hair cell motor protein. *Biophys J* **89:** 3345–3352

Okoruwa OE, Weston MD, Sanjeevi DC, Millemon AR, Fritzsch B, Hallworth R, Beisel KW (2008) Evolutionary insights into the unique electromotility motor of mammalian outer hair cells. *Evol Dev* **10:** 300–315

Oliver D, Fakler B (1999) Expression density and functional characteristics of the outer hair cell motor protein are regulated during postnatal development in rat. *J Physiol* **519:** 791–800

Oliver D, He DZ, Klocker N, Ludwig J, Schulte U, Waldegger S, Ruppersberg JP, Dallos P, Fakler B (2001) Intracellular anions as the voltage sensor of prestin, the outer hair cell motor protein. *Science* **292:** 2340–2343

Oliver D, Plinkert P, Zenner HP, Ruppersberg JP (1997) Sodium current expression during postnatal development of rat outer hair cells. *Pflügers Arch* **434:** 772–778

Oliver D, Schaechinger T, Fakler B (2006) Interaction of prestin (SLC26A5) with monovalent intracellular anions. *Novartis Found Symp* **273:** 244–253

Rajagopalan L, Patel N, Madabushi S, Goddard JA, Anjan V, Lin F, Shope C, Farrell B, Lichtarge O, Davidson AL, Brownell WE, Pereira FA (2006) Essential helix interactions in the anion transporter domain of prestin revealed by evolutionary trace analysis. *J Neurosci* **26:** 12727–12734

Reisinger E, Bresee C, Neef J, Nair R, Reuter K, Bulankina A, Nouvian R, Koch M, Buckers J, Kastrup L, Roux I, Petit C, Hell SW, Brose N, Rhee JS, Kugler S, Brigande JV, Moser T (2011) Probing the functional equivalence of otoferlin and synaptotagmin 1 in exocytosis. *J Neurosci* **31:** 4886–4895

Rybalchenko V, Santos-Sacchi J (2003) Cl- flux through a non-selective, stretch-sensitive conductance influences the outer hair cell motor of the guinea-pig. *J Physiol* **547:** 873–891

Rybalchenko V, Santos-Sacchi J (2008) Anion control of voltage sensing by the motor protein prestin in outer hair cells. *Biophys J* **95:** 4439–4447

Santos-Sacchi J (1991) Reversible inhibition of voltage-dependent outer hair cell motility and capacitance. *J Neurosci* **11:** 3096–3110

Santos-Sacchi J, Song L, Zheng J, Nuttall AL (2006) Control of mammalian cochlear amplification by chloride anions. *J Neurosci* **26:** 3992–3998

Schaechinger TJ, Oliver D (2007) Nonmammalian orthologs of prestin (SLC26A5) are electrogenic divalent/chloride anion exchangers. *Proc Natl Acad Sci USA* **104:** 7693–7698

Tan X, Pecka JL, Tang J, Okoruwa OE, Zhang Q, Beisel KW, He DZ (2011) From zebrafish to mammal: functional evolution of prestin, the motor protein of cochlear outer hair cells. *J Neurophysiol* **105:** 36–44

Xia A, Wooltorton J, Palmer D, Ng P, Pereira F, Eatock R, Oghalai J (2008) Functional prestin transduction of immature outer hair cells from normal and prestin-null mice. *JARO* **9:** 307–320

Zheng J, Long KB, Shen W, Madison LD, Dallos P (2001) Prestin topology: localization of protein epitopes in relation to the plasma membrane. *Neuroreport* **12:** 1929–1935

Zheng J, Shen W, He DZ, Long KB, Madison LD, Dallos P (2000) Prestin is the motor protein of cochlear outer hair cells. *Nature* **405:** 149–155

